Electronic Supplementary Material (ESI) for Catalysis Science & Technology.
This journal is © The Royal Society of Chemistry 2016

Mesoporous EU-1 zeolite as a highly active catalyst for ethylbenzene hydroisomerization

Electronic supplementary information

Synthesis of capping agent C_{18}-N_3-C_{18}

The multiammonium surfactant, $C_{18}H_{37}$-$N^+(CH_3)_2$-C_6H_{12}-$N^+(CH_3)_2$-C_6H_{12}-$N^+(CH_3)_2$-$C_{18}H_{37}$ (C_{18}-N_3-C_{18}), was prepared according to a procedure reported in the literature.[1] Two main components, $C_{18}H_{37}$-$N^+(CH_3)_2$-C_6H_{12}-Br and $C_{18}H_{37}$-$N^+(CH_3)_2$-C_6H_{12}-$N(CH_3)_2$, were individually prepared via alkylation of an amine with a haloalkane.

(1) *N,N'*-Dimethyloctadecane (10 mmol, 99%, TCI) and 1,6-dibromohexane (100 mmol, 99%, TCI) were dissolved in 200 ml of chloroform and heated at 333 K for 12 h. The precipitate was filtered and thoroughly washed with diethyl ether (to remove the unreacted 1,6-dibromohexane) and dried in a vacuum oven. The purity of the intermediate was analyzed by ^{1}H NMR.

(2) 1-Bromooctadecane (10 mmol, 96%, Acros Organics) and *N,N,N',N'*-tetramethyl-1,6-diaminohexane (100 mmol, 99%, TCI) were dissolved in 200 ml chloroform and heated at 333 K for 12 h. The product was separated by evaporation under vacuum. (Refrigeration aided precipitation of the product.) The solid, $C_{18}H_{37}$-$N^+(CH_3)_2$-C_6H_{12}-$N(CH_3)_2$, was then washed with diethyl ether (to remove unreacted *N,N,N',N'*-tetramethyl-1,6-diaminohexane) and dried under vacuum. The purity of the intermediate was analyzed by ^{1}H NMR.

(3) Finally, $C_{18}H_{37}$-$N^+(CH_3)_2$-C_6H_{12}-Br (10 mmol) and $C_{18}H_{37}$-$N^+(CH_3)_2$-C_6H_{12}-$N(CH_3)_2$ (10 mmol) were dissolved in chloroform and refluxed for 24 h. The solvent was evaporated under vacuum and the final product, C_{18}-N_3-C_{18}, was washed with diethyl ether and dried in a vacuum oven at 303 K. The purity of the final C_{18}-N_3-C_{18} was analyzed by ^{1}H NMR.

Detailed synthesis of B-EUO, mesoporous EUO samples, and corresponding bifunctional catalysts

For the synthesis of B-EUO, hexamethonium bromide was dissolved in an aqueous solution of NaOH. Sodium aluminate was added and the mixture was stirred till completely dissolved, after which Cab-O-Sil M5 was added. The gel was shaken for 2-3 minutes and then loaded into a Teflon-line autoclave. The mixture with the molar composition 60 SiO_2:1 Al_2O_3:5 SDA:10 Na_2O:3000 H_2O was heated with tumbling at 473 K for 60 h. The precipitated was filtered, extensively washed with distilled water, and dried at 373 K. The recovered solid was calcined under air flow (2 dm^3 g^{-1} min^{-1}) at 823 K at a cautious temperature ramp rate (1 K min^{-1}) during 20 h to effectively remove the SDA. The zeolite was then ion-exchanged four times with 1 M NH_4NO_3 aqueous solution. For the synthesis of the mesoporous EU-1 zeolites, $C_{18}H_{37}$-$N^+(CH_3)_2$-C_6H_{12}-$N^+(CH_3)_2$-C_6H_{12}-$N^+(CH_3)_2$-$C_{18}H_{37}$, here designated as C_{18}-N_3-C_{18}, was added to the conventional synthesis as a capping agent. The synthesis procedure was the same as for B-EUO. C_{18}-N_3-C_{18} was added after dissolving sodium aluminate and the mixture was stirred at 333 K until completely dissolved. Afterwards Cab-O-Sil M5 with calcined with bulk EU-1 as seeds were added as the last components. The obtained gel had a molar composition 60 SiO_2:*x*Al_2O_3:5 SDA:*y* C_{18}-N_3-C_{18}:10 Na_2O:3000 H_2O with 5 wt% of seeds towards the silica source, where *x* = 1, 0.6, 0.43 and *y* =1.0 and 1.5. The gel was heated with tumbling at 423 K for 7-10 days. The calcination and ion-exchange into NH_4^+ form was performed in the same manner as described for B-EUO. The prepared zeolites were physically mixed with γ-alumina impregnated with platinum by ion exchange with a hexachloroplatinic acid solution in the presence of 0.2 M HCl.[2,3] The hydrogenating phase (Pt/Al_2O_3) was calcined under 2 dm^3 g^{-1} min^{-1} of dry air flow at 773 K for 4 h (1 K min^{-1}).

Characterization techniques

Powder X-ray diffraction patterns were recorded with a Rigaku Multiflex diffractometer using Cu Kα radiation (40 kV, 30 mA). Scanning electron microscopy (SEM) images were obtained with a FEI VERIOS operating at 1 kV. Textural characterization was carried out in an ASAP 2020 Micromeritics instrument through argon adsorption-desorption isotherms. The surface area (S_{BET}) was evaluated by BET method using adsorption data in the P/P_0 range of 0.05-0.15. The adsorbed amount at relative pressure P/P_0 = 0.98 reflects the total adsorption capacity (V_{tot}). The NLDFT algorithm (using standard Micromeritics software for cylindrical pores for Argon on Oxides at 87 K) was used to calculate the volume of micropores (V_{mic}). S_{BJH} was calculated using BJH method with the Halsey-Faas equation. Si, Al, and Pt elemental composition was measured by inductively coupled plasma-atomic emission spectroscopy (ICP-AES) carried out on an OPTIMA 4300 DV instrument (Perkin Elmer). ^{27}Al NMR spectra were acquired in the solid state with magic angle spinning (MAS) using a Bruker Avance 400WB spectrometer at room temperature.

Adsorption of pyridine was investigated on a Nicolet 6700 spectrometer equipped with a MCT detector. Pyridine adsorption proceeded at 150 °C for 20 min at partial pressure 3 Torr, followed by 20-min evacuation at 150 °C. The concentrations of Brønsted and Lewis acid sites were calculated from integral intensities of individual bands characteristic of pyridine on Brønsted acid sites at 1545 cm^{-1} and the band of pyridine on Lewis acid sites at 1455 cm^{-1} and molar absorption coefficients of ε(B) = 1.67 ± 0.1 cm μmol^{-1} and ε(L) = 2.22 ± 0.1 cm μmol^{-1}, respectively.[4] The spectra were recorded with a resolution of 4 cm^{-1} by collection 128 scans for a single spectrum. Adsorption of DTBPy was studied on a Nicolet 6700 AEM module equipped with a DTGS detector. DTBPy adsorption proceeded at 150 °C for 15 min at equilibrium pressure 0.8 Torr, followed by 1 h degassing at the same temperature. The concentration of Brønsted acid sites was calculated from the

integral intensity of the band characteristic of DTBPy on Brønsted acid sites at 1530 cm^{-1} and a molar absorption coefficient of ε(B) = 1.67 ± 0.1 cm μmol^{-1}.

Additional characterization of B-EUO, mesoporous EUO samples and Pt/Al_2O_3

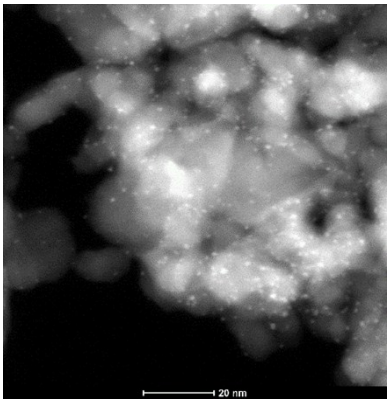

Fig. S1. STEM image of Pt dispersed on alumina. The metallic phase is present in the form of round particles with a particle size up to 1.2 nm.

The chemical composition of the initial gel was extended to evaluate the synthesis of mesoporous EUO zeolites at varying aluminum content. Two additional series with Si/Al 50 and 70 were synthesized using 1.0 and 1.5 mols of C_{18}-N_3-C_{18}. The powder XRD pattern of the first batch confirmed the presence of a pure EU-1 crystalline phase (Fig. S2a). According to ICP analysis, the samples had Si/Al 35, which was lower than their nominal value. The presence of the capping agent led to an increase in the SBJH value up to 37-58% of the total BET area.

In the sample prepared with 1.5 mols of C_{18}-N_3-C_{18}, small nanocrystals in flake-like domains were found to be similar to those in its counterpart with Si/Al 30 (Fig. S2b). Perceptible differences in the crystal and particle morphology were tentatively attributed to the varying aluminum content in the initial gel. At decreasing Al content (Si/Al 70), a clear formation of two phases in each mesoporous sample was confirmed by SEM – the bulk EUO crystals and an unknown amorphous silica phase (Fig. S2c). The narrowness of the synthetic window for EU-1 mesoporous samples is hence believed to be similar to its bulk counterpart, as reported in the literature.

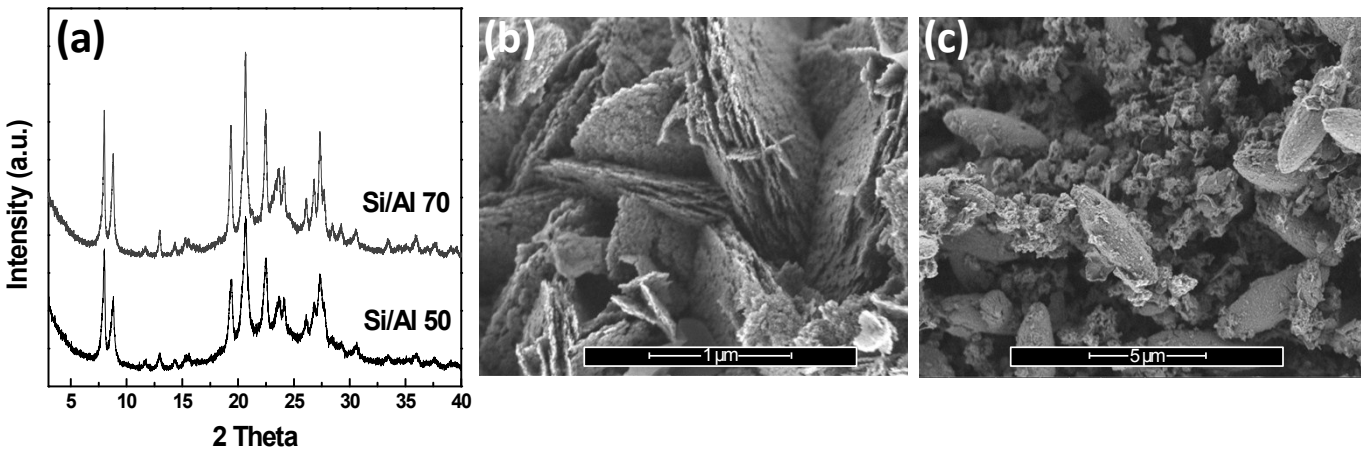

Fig. S2. Powder XRD pattern (a) and corresponding SEM images of $C_{1.5}$-EUO prepared with Si to Al molar ratios of 50 (b) and 70 (c). The presence of an additional phase in the case of Si/Al 70 is not obvious from its XRD pattern while it is striking on the SEM image, indicating the non-crystalline nature of the second phase.

Acidity Characterization

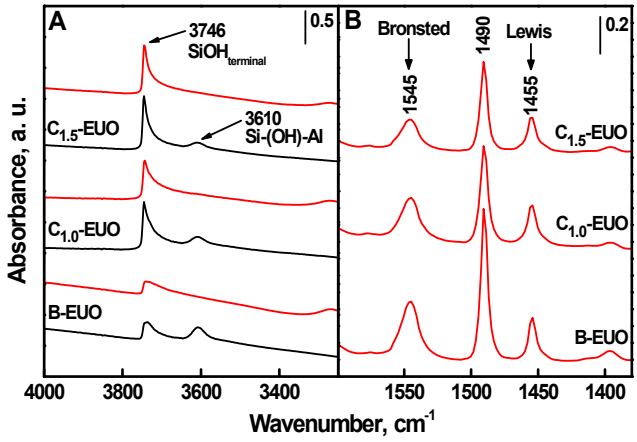

Fig. S3. Pyridine adsorption on EUO samples, (A) FTIR spectra of hydroxyl stretching region before adsorption (black spectra) and after pyridine adsorption followed by desorption (red spectra) and (B) spectra of pyridine region. Panel (B) displays the spectra after pyridine adsorption-desorption (spectra before adsorption were subtracted). All spectra are normalized to the wafer density 10 mg cm^{-2}. All three samples showed that the aluminium acid sites (Si-(OH)-Al) represented by the peak around 3610 cm^{-1} in the spectra before adsorption are accessible to the pyridine molecule because the peak completely disappeared after pyridine adsorption and desorption.

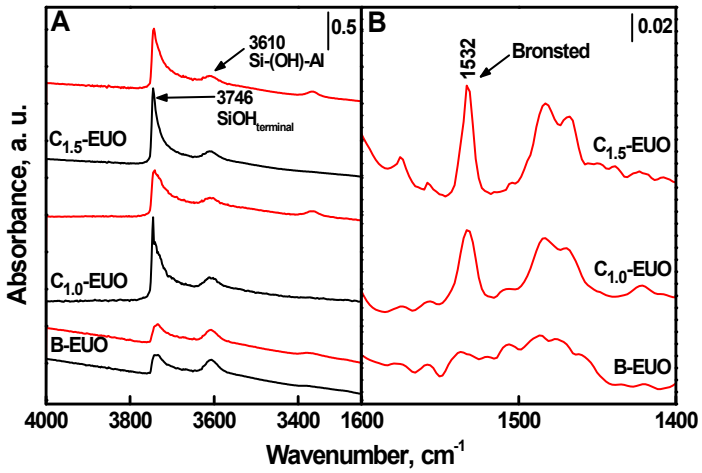

Fig. S4. DTBPy adsorption on EUO samples, (A) FTIR spectra of hydroxyl stretching region before adsorption (black spectra) and after DTBPy adsorption followed by desorption (red spectra) and (B) spectra of DTBPy region. Panel (B) displays the spectra after DTBPy adsorption-desorption (spectra before adsorption were subtracted). All spectra are normalized to the wafer density 10 mg cm^{-2}. In contrast to pyridine adsorption, large DTBPy molecules cannot enter the 10-R channels and thus interact only with the Brønsted acid sites located on the external surface and possibly in exposed 12-R side pockets. Therefore, the peak assigned to Si-(OH)-Al, aluminium acid sites, around 3610 cm^{-1} remained visible after adsorption of DTBPy for all samples as the majority of acid sites are located inside the micropores.

Table S1. Acid characterization of B-EUO and hierarchical EUO samples determined by adsorption of pyridine and 2,6-di-*tert*-butylpyridine (DTBPy) as probe molecules followed by FTIR.

Sample	Capping agent (mol)	Pyridine		DTBPy	Brønsted sites on external surface
		C_{Lewis} (µmol/g)	$C_{Brønsted}$ (µmol/g)	$C_{Brønsted}$ (µmol/g)	
B-EUO	-	92	322	8	2 %
$C_{1.0}$-EUO	1.0	100	239	37	15 %
$C_{1.5}$-EUO	1.5	87	167	49	29 %

Schematic representation of the interaction of the C_{18}-N_3-C_{18} molecules to the crystal surface

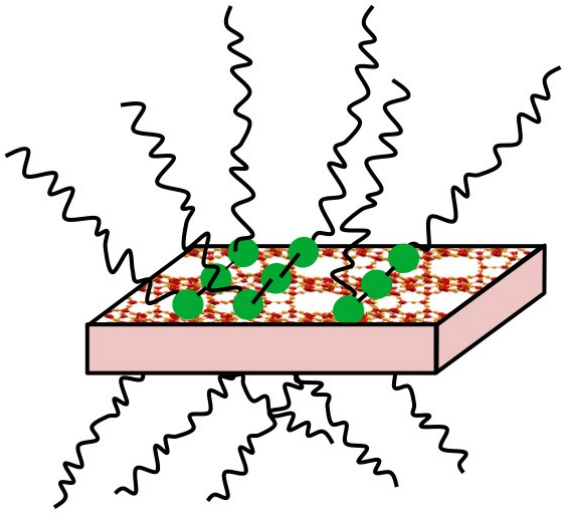

Fig. S5. Schematic representation of the synthesis of the micro-mesoporous EUO samples. The microporous network was assumed to be solely occupied by the hexamethonium bromide SDA. Conversely, the ammonium groups of the C_{18}-N_3-C_{18} molecules are believed to bind through electrostatic interactions to the crystal surface during the nucleation step.

Additional catalytic data

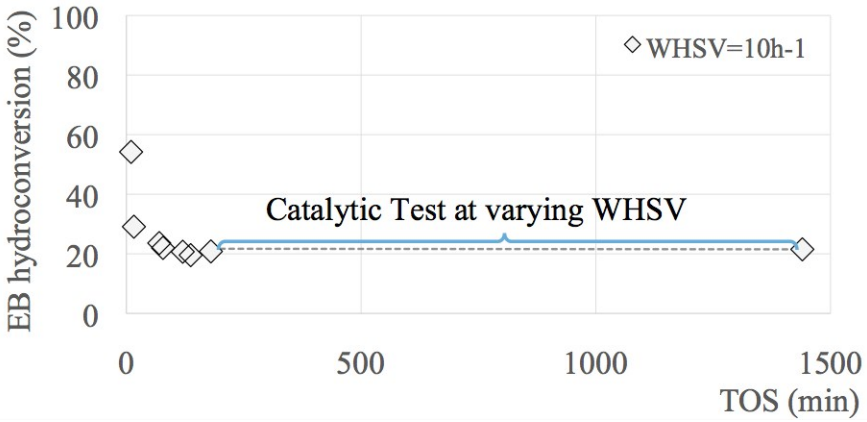

Fig. S6. Evolution of the conversion over two comparative bulk EUO samples during the stabilization period. The reproducible results of the individually tested samples confirm that the stabilization period occurs during the first 2h of reaction.

Table S2. Evaluation of the catalytic activity of each micro-mesoporous EU-1 sample, following the stabilization period and at the end of the test, at a WHSV value of $15h^{-1}$.

Sample	After stabilization	End of the catalytic test
$C_{1.0}$-EUO	25.0	24.9
$C_{1.5}$-EUO	49.5	47.5

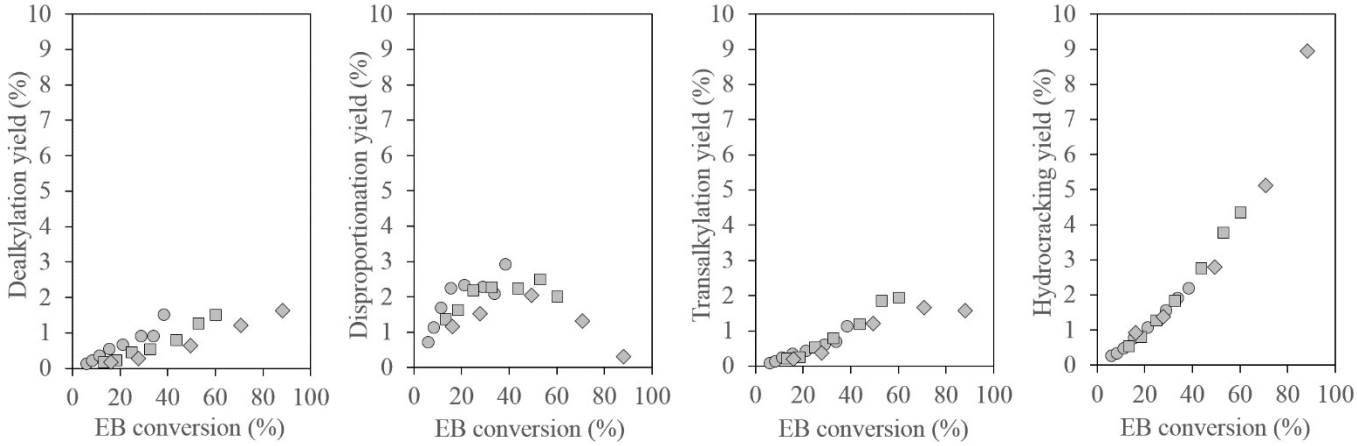

Fig. S7. Comparison of the reaction yield as a function of ethylbenzene (EB) conversion over B-EUO (○), $C_{1.0}$-EUO (◴) and $C_{1.5}$-EUO (◴). The four possible reactions that we evaluated are indicated.

References

[1] C. Jo, J. Jung, H.S. Shin, J. Kim, R. Ryoo, Capping with multivalent surfactants for zeolite nanocrystal synthesis, Angew. Chem. Int. Ed. Engl. 52 (2013) 10014–7.

[2] L.D. Fernandes, J.L.F. Monteiro, E.F. Sousa-Aguiar, A. Martinez, A. Corma, Ethylbenzene hydroisomerization over bifunctional zeolite based catalysts: The influence of framework and extraframework composition and zeolite structure, J. Catal. 177 (1998) 363–377.

[3] F. Moreau, P. Moreau, N.S. Gnep, P. Magnoux, S. Lacombe, M. Guisnet, Ethylbenzene Isomerization over Bifunctional Platinum Alumina–EUO Catalysts: Location of the Active Sites, Microporous Mesoporous Mater. 90 (2006) 327–338.

[4] B. Wichterlová, Z. Tvarůžková, Z. Sobalík, P. Sarv, Determination and properties of acid sites in H-ferrierite - A comparison of ferrierite and MFI structures, Microporous Mesoporous Mater. 24 (1998) 223–233.